



The potential of stop band material in multi-frequency ultrasonic transducers

J. Henneberg^{a,c,*}, A. Gerlach^a, H. Cebulla^b, S. Marburg^c

^a Robert Bosch GmbH, Robert-Bosch-Campus 1, 71272 Renningen, Germany

^b Technical University Chemnitz, Reichenhainer Str. 31/33, 09126 Chemnitz, Germany

^c Technical University of Munich, Boltzmann Str. 15, 85748 Garching, Germany

ARTICLE INFO

Article history:

Received 2 August 2018

Revised 6 February 2019

Accepted 31 March 2019

Available online 4 April 2019

Handling Editor: O Gottlieb

Keywords:

Multi-frequency transducer

Stop band material

Acoustic metamaterial

Band gap behavior

ABSTRACT

Ultrasonic transducers play a major role in surround sensing for automotive and industrial applications. The development of autonomous driving functions is one of the top challenges for mobility solutions of the 21st century. In this context, surround sensing systems with high performance serve as a key enabler. This leads to an increasing number of sensors which are desired to operate in parallel or in shorter intervals. Hence, measurements should be conducted with two different frequencies to discriminate the sensor signals. Known multi-frequency ultrasonic transducers mostly employ multiple electro-mechanical coupling elements which require more complex sensor electronics.

To overcome this issue, the authors present a study on multi-frequency ultrasonic transducers using only one electro-mechanical coupling element. In order to achieve suitable sound radiation properties at two well separated operating frequencies, spatially distributed stop band material is employed. As a result, the operational deflection shape can be controlled at a certain frequency. In finite element simulation, the relation between spatially distributed stop band material and the resulting operational deflection shapes is investigated. The sound radiation behavior is estimated using the numerical results from a harmonic analysis as input for the Rayleigh integral. In experimental investigations, the presented approach is validated. Finite element simulation and experimental testing show good accordance. Based on the results of the presented study, it is possible to realize a multi-frequency ultrasonic sensor with one electro-mechanical transducer element only and suitable sound radiation behavior at multiple operating frequencies.

© 2019 The Authors. Published by Elsevier Ltd. This is an open access article under the CC BY license (<http://creativecommons.org/licenses/by/4.0/>).

1. Introduction

In recent years, the development of automatic and autonomous driving function gained rising attention. This requires a more detailed and reliable surround sensing of the environment than for manual driving. Since decades, ultrasonic sensors are widely used in surround sensing applications in automotive and industrial sectors. The distance between the sensor and the object is detected by pulse-echo operation [1]. In order to get a comprehensive resolution of the environment, the number of applied ultrasonic sensors increases continuously. To operate the sensors in shorter intervals or in parallel, it is desired to use multiple operating frequencies. Thus, a signal discrimination is possible by frequency filtering.

* Corresponding author. Robert Bosch GmbH, Robert-Bosch-Campus 1, 71272 Renningen, Germany.

E-mail addresses: Johannes.Henneberg@de.bosch.com, johannes.henneberg@tum.de (J. Henneberg).

In literature, a couple of approaches to realize ultrasonic sensors with multiple operating frequencies are presented. In 1948, a stepped-frequency transducer consisting of multiple magnetostrictive nickel elements is presented by Ref. [2]. The single elements are loosely coupled to form a stack. Via a common electrical winding, the simultaneous excitation of the elements is possible. The aim of that study is to attain transducers with a broader frequency response. However, depending on the damping of the system, the approach would offer also a possibility to form multi-frequency transducers. It is found that the stepped-frequency transducers with multiple elements suffer from a lack of efficiency compared to single-frequency equivalents. In Ref. [3], a split-mode ultrasonic transducer is investigated. A structure with a two-dimensional periodicity of poled domains is created in a ferroelectric wafer with free surfaces. As a result, an ultrasonic transducer with multiple acousto-electric resonances is obtained. A piezoelectric micromachined ultrasonic transducer (PMUT) with multiple electrodes is presented in Ref. [4]. Due to multiple electrodes, the device provides high sensitivity at multiple frequencies coinciding with the first, third and fifth fundamental frequency of the transducer. Capacitive micromachined ultrasonic transducers (CMUT) are employed in Ref. [5]. A CMUT array with acoustic elements of different dimensions is designed having multiple operating frequencies. An approach using only one electro-mechanical coupling element is presented in Ref. [6]. The transmission of ultrasound is possible at multiple frequencies in the range of several MHz by adding an appropriate front layer. It is used for interstitial ultrasound thermal therapy. In the same context of medical ultrasonic therapy, a dual-frequency lead zirconate titanate (PZT)-transducer array with fundamental frequency (4.1 MHz) and third harmonic (13.3 MHz) is characterized in Ref. [7]. Ref. [8] presents a hybrid multi-frequency ultrasonic transducer. It consists of different electro-mechanical coupling elements. One of which is a piezoelectric ceramic while the other one is made of PVDF. By hybridization of both characteristic properties, the transducers enable the usage of multiple resonance frequencies. In Ref. [9], also two electro-mechanical coupling mechanisms are combined. Thus, a CMUT as well as a PMUT electro-mechanical coupling is realized in one element. The transducer can be operated at two operating frequencies. Suitable sound radiation properties for surround sensing can be expected with the obtained mode shapes at both frequencies.

However, all presented approaches suffer at least from one of the following lacks:

- The approach is not suitable for surround sensing applications. Especially the sound radiation behavior is not appropriate at various operating frequencies. It should show directivity pattern without distinctive side lobes. Hence, they are similar to monopole or dipole behavior at all operating frequencies.
- Multiple electro-mechanical coupling elements are used to realize multi-frequency transducers. This leads to more complex electronics required for surround sensing and is mostly undesired.

To overcome these issues, the present study investigates a novel approach employing spatially distributed stop band material in order to obtain a multi-frequency transducer with only one electro-mechanical coupling element and suitable sound radiation properties at two distinctive operating frequencies. Stop band materials attract attention within vibroacoustics recently [10]. Basically, it is possible to attain structures which do not allow free wave propagation in certain frequency ranges. These frequency ranges are called stop bands or band gaps [11,12]. In 2000, a phononic crystal with particular high sound transmission loss at certain frequencies is presented by Ref. [13]. The phononic crystal consists of rubber coated lead spheres which are embedded in epoxy. In Ref. [14], it is shown that stop bands caused by periodic, resonant structures show good prospect for low frequencies. Furthermore, the band gap behavior can be simply tuned by the periodic resonator. In Ref. [15], it is shown that stop bands can also be attained with randomly arranged resonant structures. However, the spacing between the resonators is required to be at a subscale of the wavelength corresponding to the desired band gap. Due to their ability to generate frequency ranges without wave propagation, stop band materials are predestined to increase sound transmission loss of structures. This is investigated in several studies, e.g. Refs. [16–22]. The possibility of waveguiding Lamb modes within a certain frequency is studied numerically and experimentally in Ref. [23]. In Ref. [24], the propagation of flexural waves in thin plates is investigated. It is shown that wave propagation can be attenuated by locally attached spring-mass resonators. The behavior of different excitations is investigated with regard to the vibration transmission. In Ref. [25], similar structures are investigated with regard to the sound transmission loss. In Ref. [26], the authors show the good prospect of stop band material in order to reduce mechanical cross-coupling in phased-array transducers.

In this study, stop band material is investigated with a rather different purpose. The operational deflection shape of a plate like structure representing a generic model of an ultrasonic transducer is modified within a certain frequency range. Therefore, sections with and without stop band behavior are spatially distributed. Stop band material shows the advantage that only a certain frequency range is effected by the particular dynamic behavior. Outside of the stop band, the influence on the dynamic behavior of the plate like structure is only small. Hence, certain operating frequencies can be tuned mainly independently from each other. This approach opens up the possibility to achieve a multi-frequency transducer having only one electro-mechanical coupling element and suitable sound radiating behavior at multiple operating frequencies. Thus, the drawback of known multi-frequency ultrasonic transducer concepts can be overcome.

This work is structured as follows: initially, we focus on the methods applied in this study. The generic model to investigate the dynamic behavior is presented in Section 3. The approach is investigated numerically with a finite element model as well as in experiments with a physical model. The results are presented in Section 4. In Section 5, the approach is transferred to the ultrasonic frequency range. Finally, a conclusion is drawn.

2. Methods

In this section, the employed methods are presented briefly. First, the Rayleigh integral is discussed in order to estimate the radiated sound pressure field generated by the plate vibration. Afterwards, the wave finite element method (WFEM) applying periodicity conditions is presented. With this approach, it is possible to characterize the wave propagation behavior in periodic structures. Finally, the experimental validation using laser Doppler vibrometer is described.

2.1. Sound radiation

The sound radiation behavior of sound transducers is usually characterized by the directivity pattern. This can be calculated in the far-field employing the Rayleigh integral [27,28]. It provides an exact solution under the following conditions:

- the radiating surface is flat,
- the radiator is embedded in a flat, infinite, and rigid baffle.

These assumptions are suitable in order to obtain a reasonable approximation of the directivity pattern for ultrasonic transducers embedded in a mounting structure like a car bumper. This is discussed in several studies like Refs. [29,30]. However, in Ref. [31] it is shown that the Rayleigh integral produces reasonable results even for more complex structures. The assumption of a baffled plate holds for the investigated structures and the ultrasonic transducers for surround sensing applications in automotive and robotic industries.

In order to fit the far-field assumption, three conditions must be fulfilled [32]. Firstly, the distance (R) between the radiator and the field point has to be much greater than the dimension (l) of the radiator

$$R \gg l. \quad (1)$$

Secondly, the condition

$$\frac{R}{l} \gg \frac{l}{\lambda} \quad (2)$$

must be fulfilled. Consequently, the error caused by phase shifts is small [33]. Finally, the wavelength (λ) should be small compared to the distance between the radiator and field point

$$\lambda \ll R. \quad (3)$$

For $e^{i\omega t}$ harmonic time dependence, the Rayleigh integral for a plane surface can be expressed by Ref. [34].

$$p(\vec{y}) = \int_{\Gamma} -i\omega\rho_f G(\vec{x}, \vec{y}) v_f(\vec{x}) d\Gamma(\vec{x}) \quad (4)$$

with

$$G(\vec{x}, \vec{y}) = \frac{e^{-ikr}}{2\pi r} \text{ and } r = |\vec{x} - \vec{y}|, \quad (5)$$

where Γ , k , ω , v_f , ρ_f , i denote the radiating surface, wavenumber, circular frequency, fluid particle velocity, fluid density, and imaginary unit. The particle velocity distribution on the surface of the structure can be used to estimate the radiated far-field sound pressure as shown in Ref. [35]. In spherical coordinates (R , ϑ , φ), the Rayleigh integral can be approximated for the sound pressure in the far-field by Ref. [32].

$$p(R, \vartheta, \varphi) = \frac{i\omega\rho_f}{2\pi R} e^{-ikR} \int_{-l_y/2}^{l_y/2} \int_{-l_x/2}^{l_x/2} e^{ik(x_Q \sin \vartheta \cos \varphi + y_Q \sin \vartheta \sin \varphi)} v(x_Q, y_Q) dx_Q dy_Q. \quad (6)$$

The transformation from Cartesian to spherical coordinates is realized by

$$\begin{aligned} x &= R \sin(\vartheta) \cos(\varphi), \\ y &= R \sin(\vartheta) \sin(\varphi), \\ z &= R \cos(\vartheta). \end{aligned} \quad (7)$$

Analyzing the directivity pattern in polar plots, it is possible to identify the sound radiation behavior of the investigated generic model.

2.2. Dispersion in periodic infinite structures

The wave propagation behavior in a periodic structure can be characterized by the dispersion relations in a unit cell. The Floquet Bloch theorem offers a possibility to handle periodic structure and to determine the wave propagation properties [36]. A freely propagating wave can be described for $e^{i\omega t}$ harmonic time dependence with angular frequency ω by

$$\psi = We^{i(\omega t - k_x x - k_y y)}, \tag{8}$$

with W describing the wave mode through the thickness of the structure, ψ being a response variable, and k_x, k_y being the components of the wavenumber in x - and y -direction, respectively. This can be obtained by employing finite element methods. The motion is described by a finite number of generalized displacements \mathbf{q} .

In case of two-dimensional periodicity in x - and y -direction, $\mathbf{q} = [\mathbf{q}_1 \ \mathbf{q}_2 \ \mathbf{q}_3 \ \mathbf{q}_4]^T$ contains the generalized displacements at nodes 1 to 4, cf. Fig. 1. The Bloch theorem states that the relation between the generalized displacements can be described by Ref. [37].

$$\begin{aligned} \mathbf{q}_2 &= \lambda_x \mathbf{q}_1, \\ \mathbf{q}_3 &= \lambda_y \mathbf{q}_1, \\ \mathbf{q}_4 &= \lambda_x \lambda_y \mathbf{q}_1, \end{aligned} \tag{9}$$

with

$$\begin{aligned} \lambda_x &= e^{-ik_x r_x} \quad \text{and} \quad \mu_x = k_x r_x, \\ \lambda_y &= e^{-ik_y r_y} \quad \text{and} \quad \mu_y = k_y r_y, \end{aligned} \tag{10}$$

where $r_{x,y}$ and $\mu_{x,y}$ represent the length of the periodic lattice and the propagation constant in the direction of periodicity, respectively. Introducing the reduction matrix by

$$\Lambda_R = [\mathbf{I} \ \lambda_x \mathbf{I} \ \lambda_y \mathbf{I} \ \lambda_x \lambda_y \mathbf{I}]^T, \tag{11}$$

the generalized displacement vector can be described dependent on \mathbf{q}_1 by

$$\mathbf{q} = \Lambda_R \mathbf{q}_1. \tag{12}$$

In the absence of damping, the generalized displacements are related to the generalized forces by

$$[\mathbf{K} - \omega^2 \mathbf{M}] \mathbf{q} = \mathbf{f}, \tag{13}$$

with \mathbf{K}, \mathbf{M} , and \mathbf{f} being the stiffness matrix, mass matrix, and force vector, respectively. Inserting Eq. (12) into Eq. (13) leads to

$$[\mathbf{K} - \omega^2 \mathbf{M}] \Lambda_R \mathbf{q}_1 = \mathbf{f}. \tag{14}$$

Assuming no external forces, the sum of nodal forces connected to node 1 is zero. Thus,

$$\Lambda_L \mathbf{f} = 0, \tag{15}$$

with

$$\Lambda_L = [\mathbf{I} \ \lambda_x^{-1} \mathbf{I} \ \lambda_y^{-1} \mathbf{I} \ \lambda_x^{-1} \lambda_y^{-1} \mathbf{I}], \tag{16}$$

can be written. Premultiplying Eq. (14) with Λ_L leads to a reduced eigenvalue problem with

$$\Lambda_L [\mathbf{K} - \omega^2 \mathbf{M}] \Lambda_R \mathbf{q}_1 = 0. \tag{17}$$

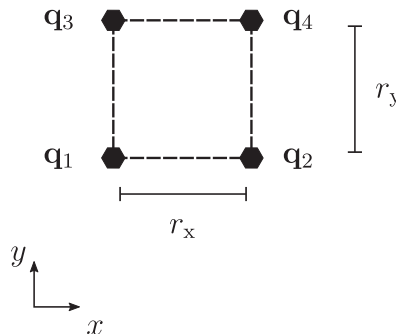


Fig. 1. Generalized displacements \mathbf{q} at various points in case of two-dimensional periodicity, based on [37].

The solution of the eigenvalue problem from Eq. (17) is a function of the propagation constants μ_x, μ_y . $\omega(\mu_x, \mu_y)$ characterizes the free wave propagation in the structure. It has to be solved for any combination of the propagation constants within the first Brillouin zone (BZ) with $\mu_x, \mu_y = [-\pi, \pi]$ [11]. Usually, the results are depicted in three-dimensional plots showing the dispersion surfaces. Thus, it is possible to identify omni-directional band gaps where no free wave propagation is possible. In case of symmetric unit cells, the calculation can be reduced to the irreducible Brillouin zone (IBZ) or to the contour of the IBZ. The three-dimensional plot of dispersion surfaces is then reduced to a two-dimensional plot of dispersion curves. This is discussed in detail in Ref. [10]. A detailed elaboration of the theory, known as wave finite element method, can be found in Refs. [37–39].

2.3. Experimental investigation

Experimental investigation is employed to validate the results of the generic model obtained from finite element simulations. In order to achieve a generic model which is comparable to a real ultrasonic transducer, fixed boundary conditions are required, cf. Section 3. These are realized by jointing the investigated structure to a backing with high stiffness and large mass compared to the structure. The velocity perpendicular to the sound radiating surface is measured at 351 scanning points with a non-contact measurement using a scanning laser Doppler vibrometer. The excitation is realized with an alternating current electric voltage of 10 V which is applied between the electrodes of the piezoelectric ceramic. Using a so called pseudo-random signal, all frequencies in the range from 0.3 kHz to 25 kHz are excited simultaneously. Furthermore, no leakage effects are introduced by this signal [40]. The obtained resonance frequencies and the related operational deflection shape (ODS) from experimental testing are then employed to validate the numerical simulations.

3. Models

In this section, the investigated models are presented. First, the generic model representing the ultrasonic transducer is discussed. The used finite element model is presented afterwards. Finally, the physical model used for experimental validation of the numerical results is described.

3.1. Generic model

A generic model is used in order to investigate the approach of using spatially distributed stop band material to attain multi-frequency transducers. It consists of a rectangular plate like structure with a sound radiating surface, a piezoelectric ceramic realizing the electro-mechanical coupling, and 112 resonators forming two sections of stop band material, cf. Fig. 2 (a) (II). The plate like structure and the resonators are made of plastics. Different configurations of the plate boundary conditions are realized with blocks of aluminum. In the first configuration CON1 only the shorter edges of the plate like structure are fixed, cf. Fig. 2 (a). This configuration is comparable to ultrasound transducers presented in Ref. [41]. A second configuration CON2 is achieved by additional, partial fixing of the long edges of the plate like structure, cf. Fig. 2 (b). Using two different configurations of the boundary conditions, it is possible to ensure that the behavior at the second operating frequency is caused by the band gap behavior of the structure. If this is the case, the second operating frequency should be mainly independent of the plate like structure boundary conditions. With regard to automotive applications, smaller and more complex transducer geometries are relevant. The authors presented a study with such geometries in Ref. [29]. However, the investigation of the generic model offers the possibility to separate the effects introduced by the stop band material from other geometrical effects. Once proofed, the principle of spatially distributed stop band material can be transferred without difficulty.

3.2. Finite element model

The dynamic behavior of the generic model is investigated in a finite element (FE) simulation. The employed model, cf. Fig. 3, consists of 20-node brick elements with quadratic interpolation functions (Element type in Abaqus: C3D20) [42]. In order to avoid mesh dependencies, the guidelines given in Ref. [43] are applied. The calculations are carried out with the commercial software Simulia Abaqus 2017. The contact between different parts is modeled as tie constraint with a surface-to-surface formulation. All materials are assumed to have linear elastic behavior according to Hooke's law. Table 1 shows the material properties applied in the FE-simulation. The piezoelectric ceramic is similar to PZT-5a [44]. Hence, the material properties are comparable to that presented in Ref. [45]. In a harmonic analysis, the forced response function is calculated. As a result, resonance frequencies can be identified. The excitation is realized by applying an electric voltage to the piezoelectric ceramic. Afterwards, the calculated surface velocity of the plate like structure is used to obtain the radiated sound field using the Rayleigh integral.

3.3. Physical model setup

The experimental validation of the approach requires a physical model, cf. Fig. 4. The plate like structure and the resonators are manufactured as a monolithic using additive manufacturing techniques. PolyJet [47] technology offers the possibility to produce fully filled, solid structures. In a following step, the piezoelectric ceramic is jointed to the downside of the plate like

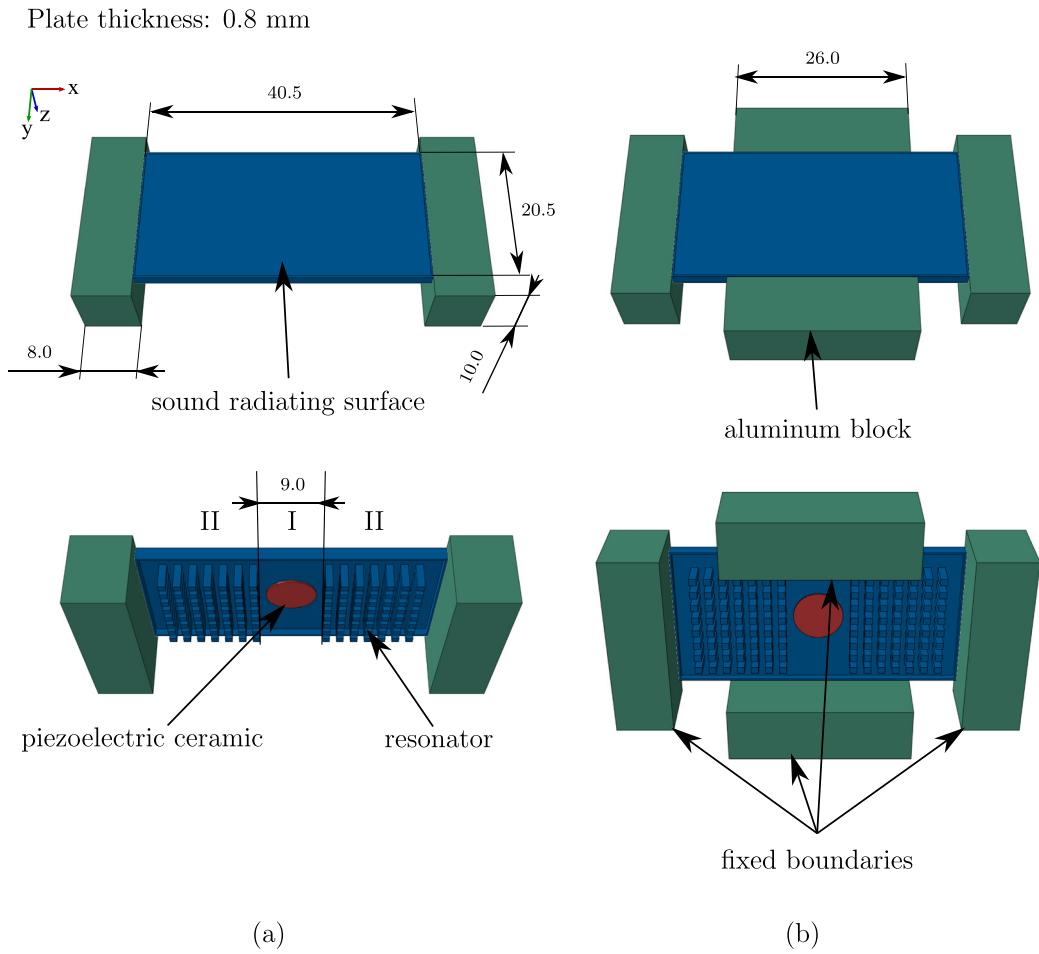


Fig. 2. Generic model to investigate the behavior of spatially distributed stop band material. It consists of a plate like structure with a middle section (I) containing the piezoelectric ceramic and two outer sections (II) with 2×56 resonators on the downside forming the stop band material. The top side of the generic model represents the sound radiating surface of an ultrasonic transducer. Two different configurations CON1 (a) and CON2 (b) are realized by assembling aluminum blocks. Thus, different boundary conditions of the plate like structure are realized. The dimensions of the generic model are given in mm.

Table 1
Material parameters of aluminum and the photopolymer VeroWhitePlus RGD 835 [46].

	VeroWhite	Aluminum
Density [$\frac{g}{cm^3}$]	1.17	2.69
Poisson's ratio [-]	0.33	0.33
Young's modulus [MPa]	3200	70000

structure. The assembly is finished by joining the aluminum blocks according to configuration CON1, cf. Fig. 2 (a), to the plate like structure. In order to realize the fixed boundaries, the entire assembly is jointed to a backing having a large mass and high stiffness compared to the plate like structure. After the experimental investigation of the test structure, additional aluminum blocks are added to the plate like structure. Hence, configuration CON2, cf. Fig. 2 (b), is realized using the same specimen. Testing one and the same structure with both configurations, allows the comparison of the results without additional influences from manufacturing and assembling of the plate like structure and the piezoelectric ceramic.

4. Results

In this section, the results obtained from the numerical simulations and experiments are presented. First, the operational deflection shapes of the two configurations are compared. The sound radiation behavior at certain resonance frequencies is depicted using polar plots. Finally, the numerical results are validated by experimental results. Therefore, the ODSs between

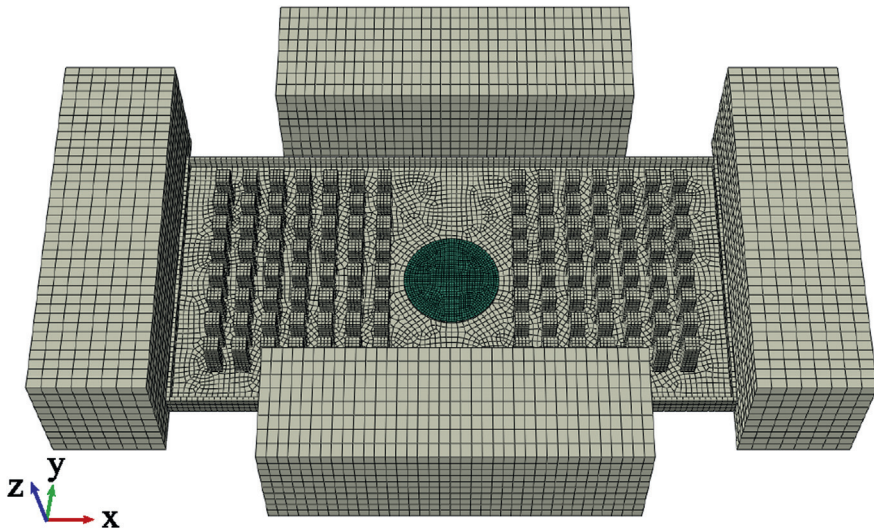


Fig. 3. Finite element model of configuration CON2. It consists of 20 node brick elements with quadratic interpolation functions.

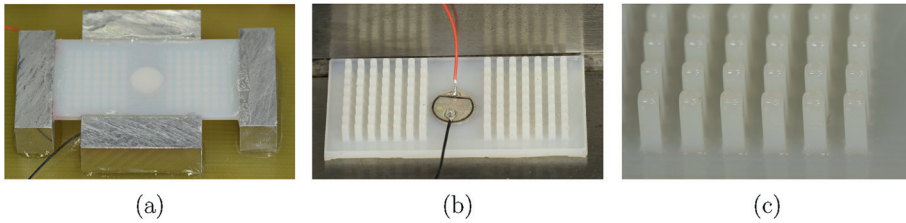


Fig. 4. Physical model for experimental validation. (a) Assembly of the configuration CON2 with fixed boundary conditions at all edges. (b) Downside of the plate like structure with resonators as one part and jointed piezoelectric ceramic in the center. (c) Detailed view of resonators.

numerical simulations and experiments are compared.

4.1. Operational deflection shape and stop band behavior

The operational deflection shape of the plate surface characterizes the sound radiation behavior. In order to generate the desired directivity pattern with small side lobes, the ODS should be similar to the first normal mode. This could be either the

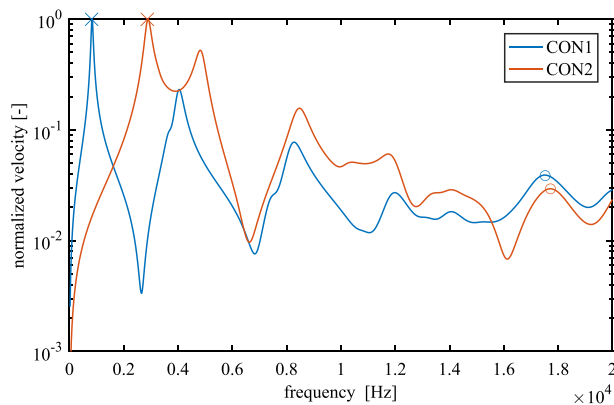


Fig. 5. Frequency response function of normalized velocity at the center point of the sound radiating surface. First and second operating frequencies are identified by \times and \circ , respectively. The first operating frequency is influenced by the boundary conditions. In contrary, the second one is mainly independent of the additional boundary conditions in configuration CON2. Other peaks in the frequency response function correspond to ODSs which do not show suitable sound radiation behavior for surround sensing purposes.

entire structure or only a part of the structure while the rest remains in equilibrium position. Achieving the first case is rather trivial. The operating frequency coincides with the first eigenfrequency of the plate like structure. Due to the different boundary conditions in configurations CON1 and CON2, the lowest operating frequencies are obtained at 0.83 kHz and 2.9 kHz, respectively. These can be identified in the frequency response function (FRF) shown in Fig. 5 highlighted by \times . The corresponding ODSs are depicted in Fig. 6.

An ODS where a part of the structure behaves similar to the first normal mode while the rest remains in equilibrium position is achieved at higher frequencies. This frequency is highlighted by \circ in Fig. 5 for each configuration. At 17.5 kHz and 17.7 kHz in configurations CON1 and CON2, respectively, the middle section of the plate like structure shows an ODS where almost all nodes move with the same phase. The outer sections, consisting of stop band material, remain almost without displacement, cf. Fig. 6. The additional boundary conditions in configuration CON2 have only small influence on the resulting operating frequency. Hence, the operating frequency OF2 is mainly independent of the additional boundary conditions. This ODS seems suitable to serve as a second operating point. The ODS of both configurations are pretty similar. However, at the boundary of the plate like

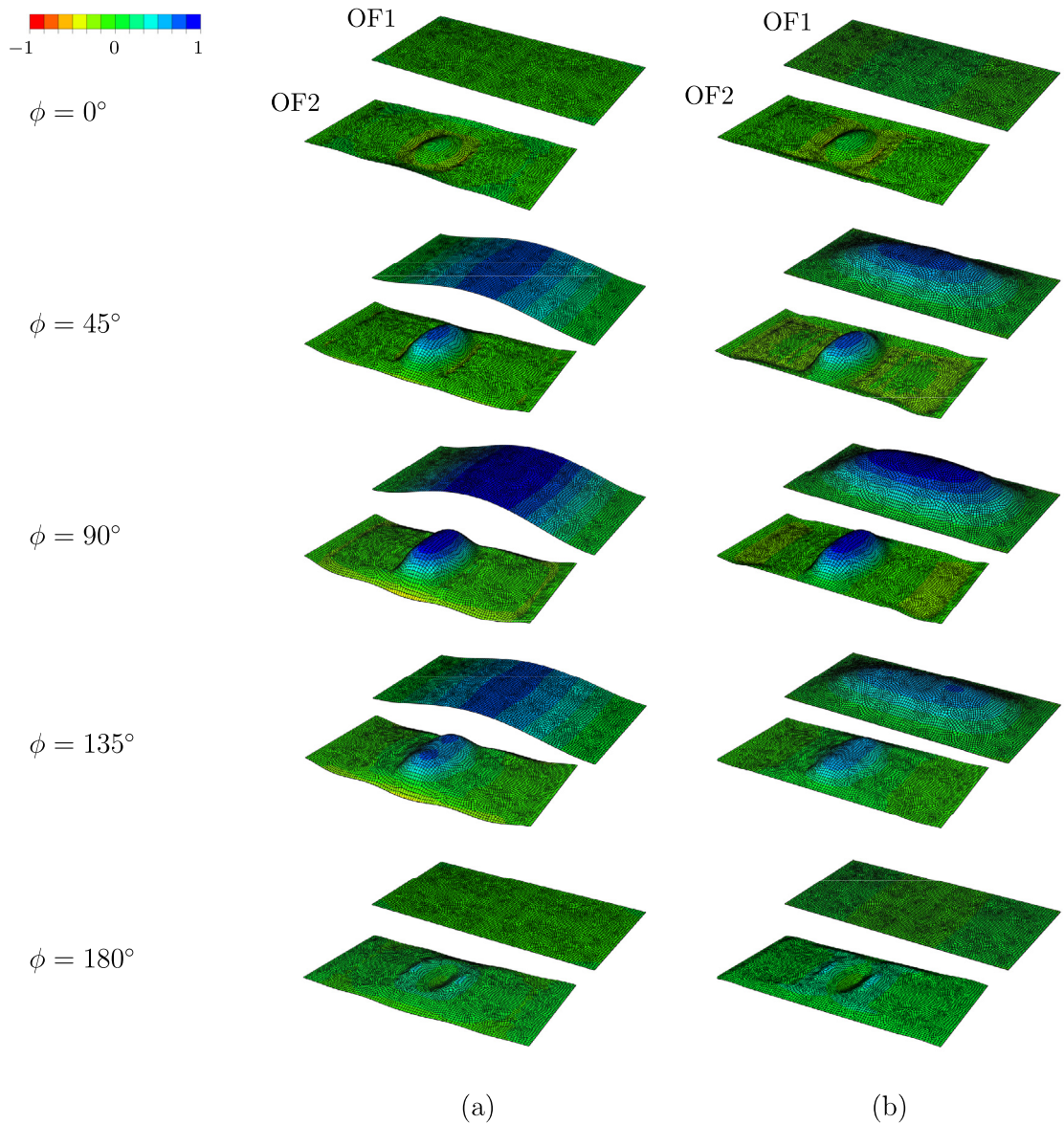


Fig. 6. Operational deflection shape at first (OF1) and second operating frequency (OF2) of the sound radiating surface obtained from finite element simulation. The coloring shows the normalized displacement perpendicular to the undeformed surface. For a better understanding, the phase angles are shown from 0° to 180° in steps of 45° . In case of the second operating frequency, the operational deflection shapes are similar in configuration CON1 (a) and configuration CON2 (b) at all phase angles ϕ . The middle section shows high displacement while the outer sections remain almost in equilibrium position.

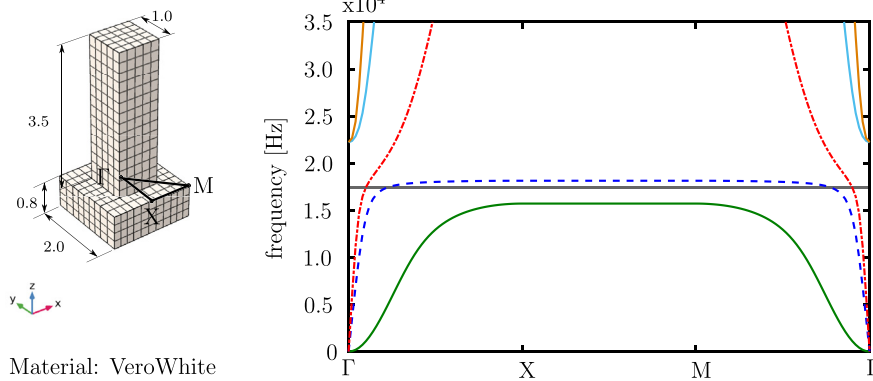


Fig. 7. Unit cell of the stop band material and dispersion curves to identify stop bands for configurations CON1 and CON2. The dispersion curves are related to different wave types. Stop band behavior is found for shear waves (— —) and bending waves (—). Longitudinal waves (---) can pass the unit cell at all frequencies. The dimensions of the unit cell are given in mm.

structure a difference in the ODS can be found. This is due to the missing boundary conditions in configuration CON1.

In order to characterize the band gap behavior of the outer plate sections, the dispersion curves are investigated. Fig. 7 shows the unit cell consisting of a plate like structure and a beam with quadratic cross-section. In order to identify band gaps, the propagation constants are set to fit the contour of the IBZ $\Gamma X M$ [11]. This is suitable due to the symmetry of unit cell as shown in Ref. [10]. The dispersion diagram shows that a partial stop band is achieved with this type of band gap material. In Ref. [26], a similar unit cell is investigated. It is shown that a band gap is obtained for shear (— —) and bending waves (—) while longitudinal waves (---) can pass the unit cell at all frequencies, cf. Fig. 7.

It is found that the second operating frequency of the transducer emerges within the stop band where bending waves can not propagate freely through the outer section of the plate like structure. Consequently, the behavior of the plate like structure at the second operating frequency can be interpreted as follows:

A harmonic dynamic excitation of the plate like structure is introduced in the center using the piezoelectric ceramic. The excitation frequency coincides with the stop band frequency of outer section. Due to the particular dynamic behavior of this section, the bending wave is reflected at the boundary of the stop band material. Thus, the dynamic behavior mainly depends on the stop band material.

4.2. Directivity patterns

The sound radiation behavior is a criterion to assess the usability of the presented approach to achieve multi-frequency transducers. The directivity pattern should exhibit an even form without distinctive side lobes. Hence, they are desired to behave similar to monopole or dipole characteristics. The directivity pattern is obtained applying the Rayleigh integral to the sound radiating surface of the generic model. The visualization is usually done in polar plots, cf. Fig. 8. At the first operating frequency, both configurations radiate sound without any side lobes. The directivity patterns at the second operating frequency differ slightly between the two configurations. In case of configuration CON1, the sound pressure level shows a drop to -6 dB in x -direction at the center point. In configuration CON2, this drop is reduced to -3 dB. This can be ascribed to lower displacements of the structure at the outer sections due to the additional boundary conditions. In y -direction, configuration CON1 shows monopole behavior. In contrast, a characteristic similar to a dipole is found in configuration CON2 in y -direction. In this case, the sound pressure levels shows a drop to -14 dB at an angle of $\pm 71^\circ$. However, in test both cases the directivity pattern does not show distinctive side lobes.

4.3. Experimental results

From experimental testing, the resonance frequencies and the related ODS are obtained. Comparing these results with results from numerical simulation, it is possible to validate the employed FE-model. Table 2 shows the operating frequency from FE-simulation and experimental testing. Regarding the first operating frequency, the deviation between simulation and experiment is less than 4% in both configurations. Thus, a suitable accuracy of the applied finite element model is validated.

Considering the second operating frequency, the deviation from numerical results increases to almost 15%. However, the ODSs of the second operating frequency exhibit equal behavior in FE-simulation and experimental testing, cf. Fig. 9. As the second operating frequency is equal for both configurations CON1 and CON2, it is experimentally proved that the additional fixation of the plate like structure has no influence on the second operating frequency for in the investigated configurations.

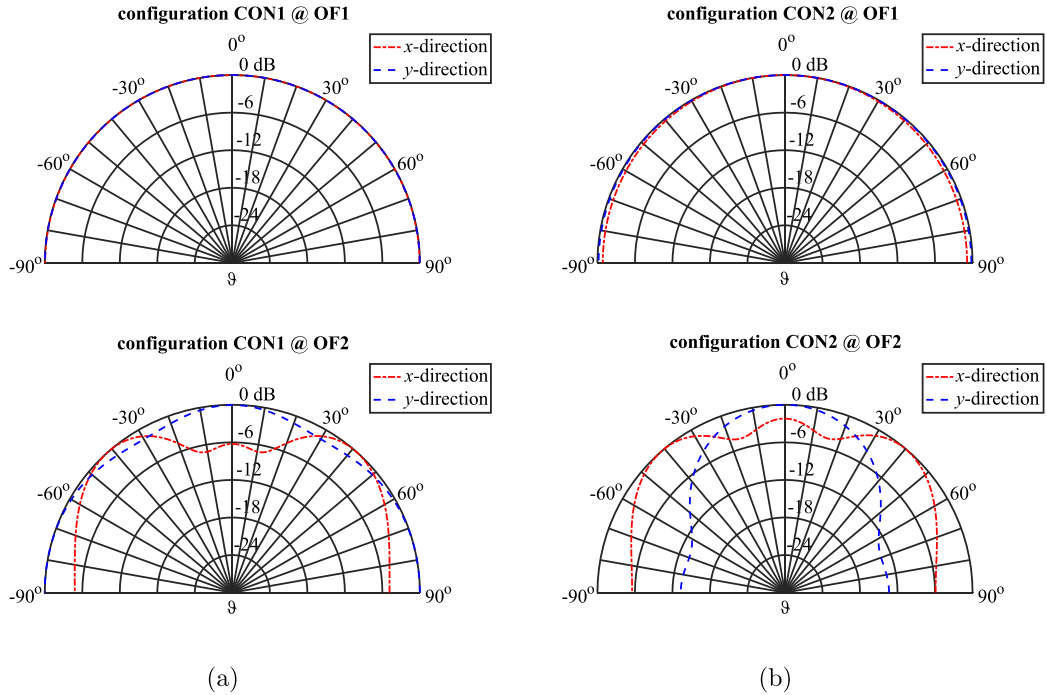


Fig. 8. Directivity patterns of configurations CON1 (a) and CON2 (b) at the first (OF1) and second (OF2) operating frequency. The polar plots show the sound pressure level in x- and y-direction which are defined by $\varphi = 0^\circ$ and $\varphi = 90^\circ$, respectively.

Table 2
Results from numerical simulation and experiment.

		Simulation [kHz]	Experiments [kHz]
CON1	1 st operational frequency	0.83	0.8
	2 nd operational frequency	17.5	20.1
CON2	1 st operational frequency	2.9	2.8
	2 nd operational frequency	17.7	20.2

4.4. Discussion

Summarizing the results, the dynamic behavior can be divided into two categories. In the first category, the excitation frequency does not coincide with the frequency of the stop band. In this case, the vibrational behavior of the plate like structure is similar to that known from classical plate theory. Thus, the boundary conditions have significant influence on the resonance frequencies and the corresponding ODSs. In the second category, the excitation frequency is in the range of the stop band. In this case, a particular dynamic behavior of the system is found. This leads to ODSs where a part of the structure behaves similar to the first normal mode while the rest remains in equilibrium position. The behavior can be interpreted as follows. The wave is excited by the piezoelectric ceramic. In section 1, the wave is freely propagated. In contrast, no free wave propagation is possible in section 2 due to the coincidence of the excitation frequency and the frequency range of the stop band. Thus, the wave gets reflected at the edge of section 2. Hence, it becomes clear that the operating frequency OF2 is found within the frequency range of the stop band for bending waves. By the geometrical design of zone I, the resulting ODS as well as the operating frequency laying within the stop band can be adjusted.

Investigating two different configurations, it is shown that the effect is caused by the stop band behavior of the structure rather than by the boundary conditions. These findings could also be transferred to other applications where certain dynamic behavior is desired independently from the boundary conditions. Hence, the same design could be used in various applications without influencing the dynamic behavior. In the present test case, this effect leads to a suitable sound radiation for both configurations. The results of the directivity pattern in this study must be seen in the context of the generic model. As the directivity pattern strictly depends on the operating frequency and the dimensions of the radiator, the results of the generic model can not be transferred directly to real transducer applications. However, the results are suitable to estimate the potential of spatially distributed stop band material. Due to the additional boundary conditions in

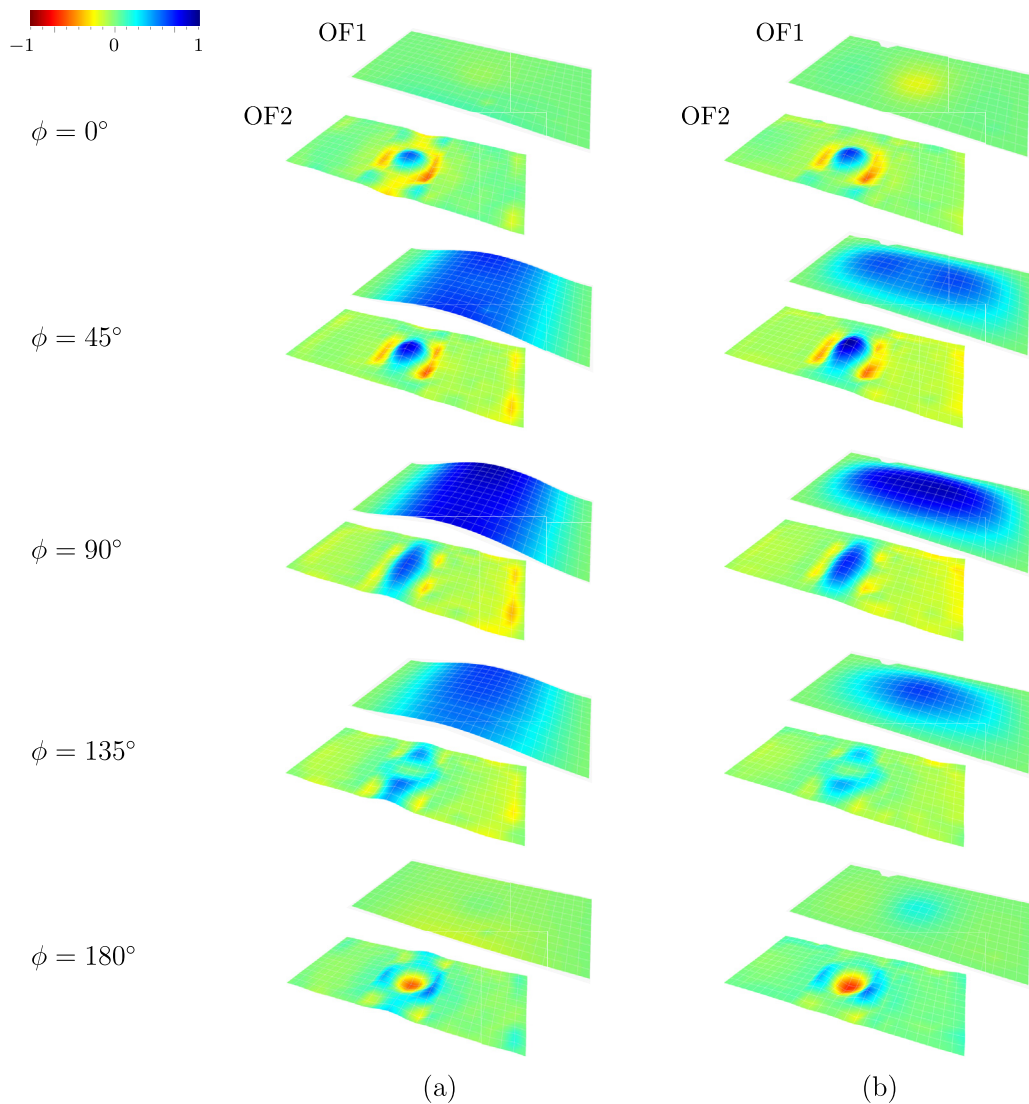


Fig. 9. Operational deflection shape at first (OF1) and second operating frequency (OF2) of the sound radiating surface obtained from experimental testing. The results are similar to that presented in Fig. 6. The coloring shows the normalized displacement perpendicular to the undeformed surface. For a better understanding, the phase angles are shown from 0° to 180° in steps of 45° . In case of the second operating frequency, the operational deflection shapes are similar in configurations CON1 (a) and CON2 (b) at all phase angles ϕ . The middle section shows high displacement while the outer sections remain almost in equilibrium position.

configuration CON2, a more even directivity pattern is obtained. Hence, this configuration is more suitable to build multi-frequency ultrasonic transducers. In order to achieve more even directivity patterns at the second operating frequency, fixed boundary conditions along all edges should be considered. The investigation shows that the operating frequencies are not coupled to each other. Hence, it is possible to tune the operating frequencies mainly independently from each other.

Furthermore, the piezoelectric ceramic could be surrounded entirely by stop band material. In this case, the waves would be reflected as well when traveling in y -direction which would reduce the displacement of the outer section of the plate like structure. As a result, this would generate a more even directivity pattern. Employing the presented approach, it would be possible to achieve ultrasonic transducers with more than two operating frequencies. Therefore, various types of stop band material should be spatially distributed. Exhibiting stop bands at different frequency bands, multiple operating frequencies could be achieved with suitable sound radiation behavior. In experimental investigation, the results from numerical simulation are validated. Good accordance is found for the first operating frequency in both configurations. The second operating frequency obtained in experimental testing shows higher deviation from the simulation results. This can be ascribed to a lack of accuracy in additive manufacturing processes resulting in resonators with a larger cross-section at the plate side and smaller cross-section at the free end, cf. Fig. 4 (c). Consequently, the center frequency of the stop band is increased in experimental testing in comparison

Plate thickness: 0.8 mm

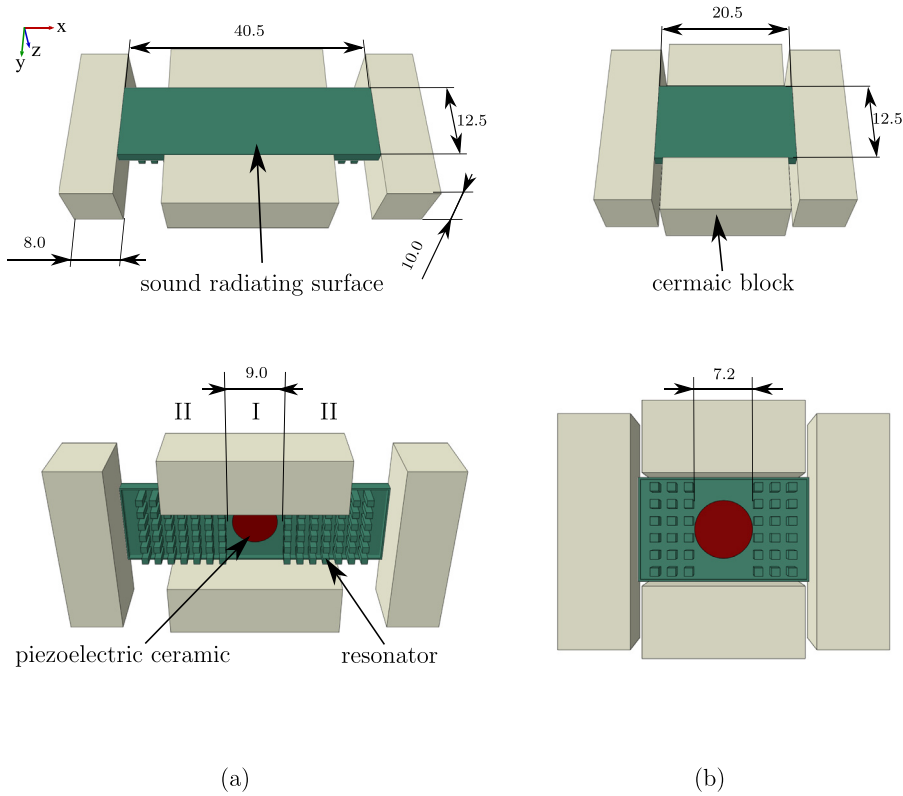


Fig. 10. Models of ultrasonic transducers with multiple operating frequencies in ultrasonic range. (a) CON3 with dimensions similar to the dimensions of the generic model, cf. Fig. 2. (b) CON4 with reduced length in x -direction and reduced width of section 1. The dimensions of the models are given in mm.

to numerical simulation. Finally, this results in an increased second operating frequency. However, the comparison of the ODSs from numerical simulation and experimental testing shows good accordance for both configurations. It is shown that spatially distributed stop band material is a suitable approach to achieve multi-frequency ultrasonic transducers. Thus, it is possible to overcome the drawbacks of known multi-frequency ultrasonic transducer concepts.

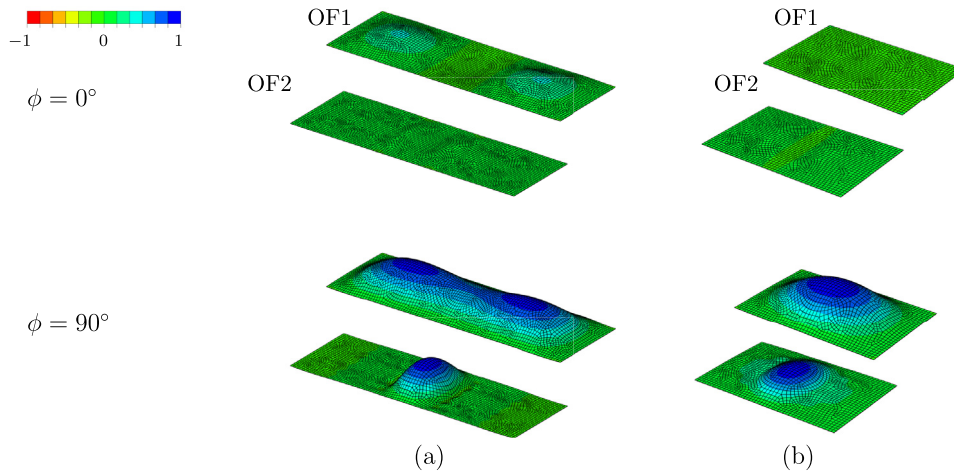


Fig. 11. Operational deflection shape at first (OF1) and second operating frequency (OF2) of the sound radiating surface obtained from finite element simulation. The coloring shows the normalized displacement perpendicular to the undeformed surface. For the sake of brevity, only the phase angles 0° and 90° are shown.

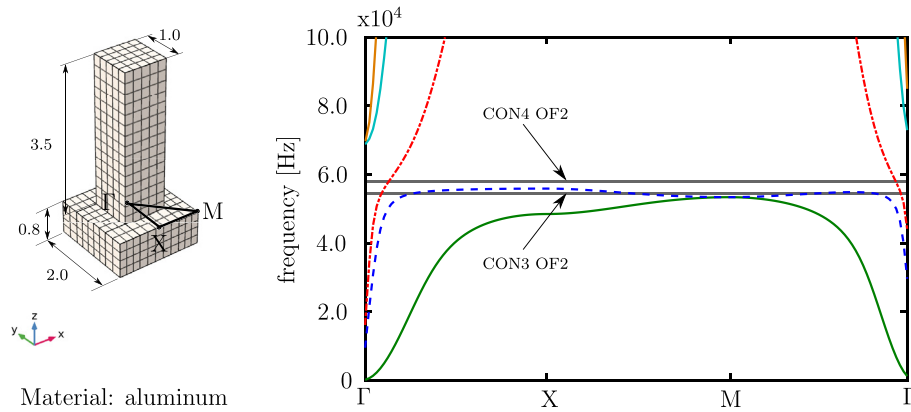


Fig. 12. Unit cell of the stop band material and dispersion curves to identify stop bands for configuration CON3 and CON4. The dispersion curves are related to different wave types. Stop band behavior is found for shear waves (---) and bending waves (—). Longitudinal waves (-.-) can pass the unit cell at all frequencies. The dimensions of the unit cell are given in mm.

5. Transfer to ultrasonic frequency range

For practical use, the previously presented results need to be transferred to the ultrasonic frequency range. This can be achieved by changing the material as well as by adjusting the geometry of the transducer. In this section, two additional configurations are presented with both operating frequencies in the ultrasonic range (> 16 kHz [48]). Configurations CON3 and CON4 are introduced in Fig. 10.

In contrast to CON1 and CON2, the configurations for the ultrasonic frequency range are made of aluminum. Due to the high ratio from Young's modulus to mass density, the operating frequency increases compared to the previous configurations which were made of plastics. In order to realize proper boundary conditions of the plate like structure, the blocks are considered to consist of ceramic material. The geometrical design of configuration CON3 is similar to the one of CON2. Only the plate width in y -direction is reduced and the corresponding resonators are removed. This is necessary to ensure that the ODS of a part of

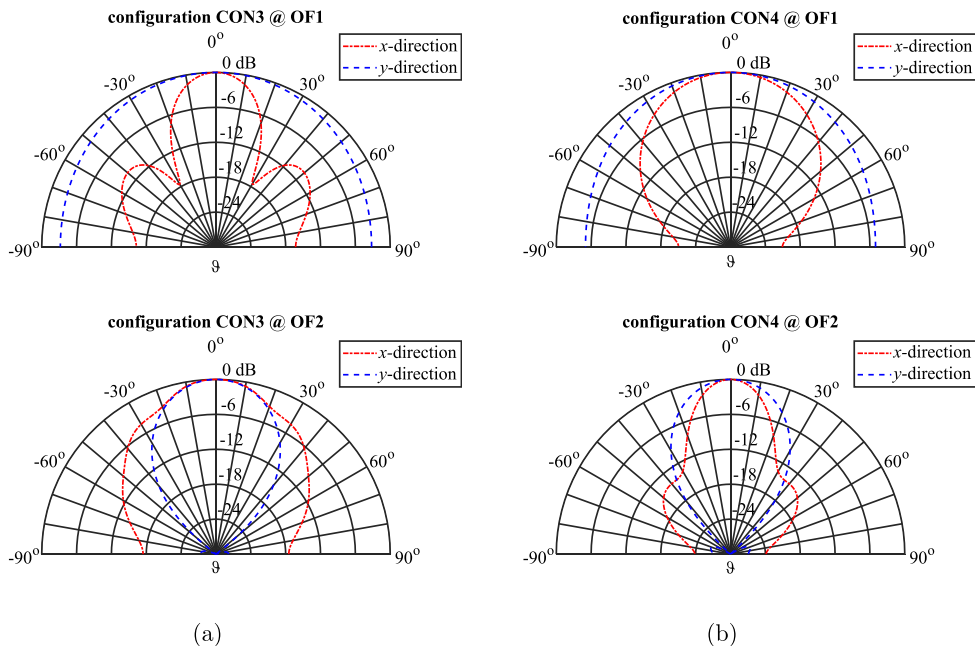


Fig. 13. Directivity patterns of configurations CON3 (a) and CON4 (b) at the first (OF1) and second (OF2) operating frequency. The polar plots show the sound pressure level in x - and y -direction which are defined by $\varphi = 0^\circ$ and $\varphi = 90^\circ$, respectively.

the structure behaves similar to the first normal mode if the OF2 is increased. In configuration CON4, the length of the plate in x -direction is reduced additionally and the corresponding resonators are removed. Thus, the OF1 is increased.

The operational deflection shapes of both operating frequencies are shown in Fig. 11. OF1 arises at 18.9 kHz and 23.7 kHz for CON3 and CON4, respectively. The second operating frequency OF2 is achieved at 55.2 kHz and 58.5 kHz for CON3 and CON4, respectively. Thus, the results found for the generic model in the previous sections can be reproduced numerically also in the ultrasonic range. Fig. 12 shows the dispersion curves for the configurations CON3 and CON4. OF2 coincides with the stop band for bending waves in a similar way as found in the generic model. The dimensions of zone I are different in configurations CON3 and CON4. As a result, the second operating frequency OF2 differs between configurations CON3 and CON4. However, both are found in the frequency range of the stop band for the bending waves. The resulting directivity patterns show suitable sound radiation behavior for the use in surround sensing applications, cf. Fig. 13. Thus, it is shown, that spatially distributed stop band material is a suitable approach to achieve multi-frequency ultrasonic transducers.

6. Conclusion

A study on multi-frequency ultrasonic transducers with spatially distributed stop band material has been presented. The desired ultrasonic transducer is required to work at different operating frequencies using only one electro-mechanical coupling element. The directivity pattern of the radiated sound field needs to be even and should not show distinctive side lobes. In a generic model, the effect of spatially distributed stop band material is investigated in order to fulfill these requirements. The approach is studied with different boundary conditions of the generic model. Finite element simulation is employed to identify the operating frequencies and the belonging ODSs. The results are used to calculate the directivity pattern of the radiated sound field using the Rayleigh integral. In experimental testing, the results of the numerical simulation are validated. The obtained ODSs show good accordance between simulation and experiment.

The authors conclude that:

- (i) spatially distributed stop band material is identified as a suitable solution to achieve multi-frequency ultrasonic transducers using only one electro-mechanical coupling element,
- (ii) the second operating frequency is related to the frequency of the stop band,
- (iii) the second operating frequency achieved by the introduction of spatially distributed stop band material and the belonging ODSs are mainly independent of additional boundary conditions in configurations CON1 and CON2,
- (iv) suitable sound radiation behavior is achieved at two well separated operating frequencies, and
- (v) distinctive operating frequencies can be tuned mainly independently from each other.

The presented approach offers a possibility to design multi-frequency ultrasonic transducers with only one electro-mechanical coupling element and suitable sound radiation properties at the same time. Thus, the previously discussed drawbacks of known concepts can be overcome. This is a major contribution to increase the surround sensing performance and reliability of ultrasonic transducers.

Acknowledgements

The authors gratefully acknowledge Robert Bosch GmbH Germany for the funding of this research.

Appendix A. Supplementary data

Supplementary data to this article can be found online at <https://doi.org/10.1016/j.jsv.2019.03.026>.

References

- [1] R. Lerch, G. Sessler, D. Wolf, *Technische Akustik: Grundlagen und Anwendungen (Technical acoustics: Basics and applications)*, Springer Berlin Heidelberg, 2009.
- [2] F.P. Bundy, Characteristics of stepped-frequency transducer elements, *J. Acoust. Soc. Am.* 20 (3) (1948) 297–304.
- [3] I. Ostrovskii, L. Cremaldi, Split-mode ultrasonic transducer, *J. Acoust. Soc. Am.* 134 (2) (2013) 1715–1723.
- [4] T. Wang, C. Lee, Electrically switchable multi-frequency piezoelectric micromachined ultrasonic transducer (pmut), in: 2016 IEEE 29th International Conference on Micro Electro Mechanical Systems (MEMS), 2016, pp. 1106–1109.
- [5] M. Maadi, R.J. Zemp, Self and mutual radiation impedances for modeling of multi-frequency CMUT arrays, *IEEE Trans. Ultrason. Ferroelectr. Freq. Contr.* 9 (9) (2016) 1441–1454.
- [6] R. Chopra, C. Luginbuhl, F.S. Foster, M.J. Bronskill, Multifrequency ultrasound transducers for conformal interstitial thermal therapy, *IEEE Trans. Ultrason. Ferroelectr. Freq. Contr.* 50 (7) (2003) 881–889.
- [7] M. Burtnyk, W.A. N'Djin, L. Persaud, M. Bronskill, R. Chopra, Acoustic characterization of multi-element, dual-frequency transducers for high-intensity contact ultrasound therapy, *AIP Conf. Proc.* 1481 (1) (2012) 26–31.
- [8] I. Muttakin, S.M. Nooh, E. Supriyanto, Spice modeling of hybrid multi-frequency ultrasound transducer, in: Proceedings of the 10th WSEAS International Conference on System Science and Simulation in Engineering, World Scientific and Engineering Academy and Society (WSEAS), Stevens Point, Wisconsin, USA, 2011, pp. 106–111.
- [9] C. Sun, F. Dai, S. Jiang, Y. Liu, A novel single-element dual-frequency ultrasound transducer for image-guided precision medicine, in: 2017 IEEE International Ultrasonics Symposium (IUS), 2017, pp. 1–4.

- [10] F. Maurin, C. Claeys, E. Deckers, W. Desmet, Probability that a band-gap extremum is located on the irreducible Brillouin-zone contour for the 17 different plane crystallographic lattices, *Int. J. Solids Struct.* 135 (2018) 26–36.
- [11] L. Brillouin, *Wave Propagation in Periodic Structures: Electric Filters and Crystal Lattices*, Dover Publications, 1953.
- [12] Z.-J. Yao, G.-L. Yu, Y.-S. Wang, Z.-F. Shi, Propagation of bending waves in phononic crystal thin plates with a point defect, *Int. J. Solids Struct.* 46 (13) (2009) 2571–2576.
- [13] Z. Liu, X. Zhang, Y. Mao, Y.Y. Zhu, Z. Yang, C.T. Chan, P. Sheng, Locally resonant sonic materials, *Science* 289 (5485) (2000) 1734–1736.
- [14] C.C. Claeys, K. Vergote, P. Sas, W. Desmet, On the potential of tuned resonators to obtain low-frequency vibrational stop bands in periodic panels, *J. Sound Vib.* 323 (2013) 1418–1436.
- [15] M. Rupin, F. Lemoult, G. Lerosey, P. Roux, Experimental demonstration of ordered and disordered multiresonant metamaterials for Lamb waves, *Phys. Rev. Lett.* 112 (2014) 234301.
- [16] C.C. Claeys, P. Sas, W. Desmet, On the acoustic radiation efficiency of local resonance based stop band materials, *J. Sound Vib.* 333 (2014) 32033213.
- [17] Y. Song, L. Feng, J. Wen, D. Yu, X. Wen, Reduction of the sound transmission of a periodic sandwich plate using the stop band concept, *Compos. Struct.* 128 (2015) 428–436.
- [18] B. Assouar, M. Oudich, X. Zhou, Acoustic metamaterials for sound mitigation, *C. R. Phys.* 17 (5) (2016) 524–532 (phononic crystals/Cristaux phononiques).
- [19] C. Claeys, E. Deckers, B. Pluymers, W. Desmet, A lightweight vibro-acoustic metamaterial demonstrator: numerical and experimental investigation, *Mech. Syst. Signal Process.* 70 (2016) 853–880.
- [20] H. Ruiz, C. Claeys, E. Deckers, W. Desmet, Numerical and experimental study of the effect of microslits on the normal absorption of structural metamaterials, *Mech. Syst. Signal Process.* 70–71 (2016) 904–918.
- [21] X. Wang, H. Zhao, X. Luo, Z. Huang, Membrane-constrained acoustic metamaterials for low frequency sound insulation, *Appl. Phys. Lett.* 108 (4) (2016) 041905.
- [22] N.G. Rocha de Melo Filho, L. Sangiuliano, C. Claeys, E. Deckers, W. Desmet, Vibro-acoustic metamaterials for increased STL in acoustic resonance driven environments, in: *Proceedings: Noise and Vibration Emerging Methods*, 2018, p. 13. no. 171978.
- [23] T.-C. Wu, T.-T. Wu, J.-C. Hsu, Waveguiding and frequency selection of Lamb waves in a plate with a periodic stubbed surface, *Phys. Rev. B* 79 (2009) 104306.
- [24] Y. Xiao, J. Wen, X. Wen, Flexural wave band gaps in locally resonant thin plates with periodically attached spring-mass resonators, *J. Phys. D Appl. Phys.* 45 (19) (2012) 195401.
- [25] Y. Xiao, J. Wen, X. Wen, Sound transmission loss of metamaterial-based thin plates with multiple subwavelength arrays of attached resonators, *J. Sound Vib.* 331 (25) (2012) 5408–5423.
- [26] J. Henneberg, A. Gerlach, H. Storck, H. Cebulla, S. Marburg, Reducing mechanical cross-coupling in phased array transducers using stop band material as backing, *J. Sound Vib.* 424 (2018) 352–364.
- [27] J.W. Baron Rayleigh Strutt, *The Theory of Sound*, vol. 2, Dover Publications, 1896.
- [28] G.H. Koopmann, J.B. Fahnlne, *Designing Quiet Structures: A Sound Power Minimization Approach*, Elsevier Science, 1997.
- [29] J. Henneberg, A. Gerlach, H. Cebulla, S. Marburg, Locally structured fiber reinforcements: an approach to realize anisotropic directivity pattern in ultrasound transducers, in: *SAE Technical Paper*, No. 2018-01-1485, SAE International, 2018, p. 13.
- [30] C.-C. Cheng, C.-Y. Lin, W.-J. Wu, K.-C. Wu, C.-K. Lee, Highly anisotropic beam patterns for a pot-like ultrasonic sensor with penetrating slots configuration, in: *2009 IEEE International Ultrasonics Symposium*, 2009, pp. 775–778.
- [31] D. Fritze, S. Marburg, H.-J. Hardtke, Estimation of radiated sound power: a case study on common approximation methods, *Acta Acustica United Acustica* 95 (5) (2009) 833–842.
- [32] M. Möser, *Technische Akustik (Technical Acoustics)*, tenth ed., Springer-Verlag, Berlin Heidelberg New York, 2015.
- [33] M. Möser, *Engineering Acoustics: an Introduction to Noise Control*, second ed., Springer, 2009.
- [34] S. Marburg, Developments in structural-acoustic optimization for passive noise control, *Arch. Comput. Methods Eng.* 9 (4) (2002) 291–370.
- [35] G. Hübner, A. Gerlach, Zusammenhang der DFEM-Schalleistungsbeschreibung mit der Rayleighschen Schallfelddarstellung ebener Strahler (The relation between DFEM sound power description and Rayleigh sound field depicting of plane sound sources), in: *Fortschritte der Akustik/DAGA*, 1998, pp. 682–683.
- [36] F. Bloch, Über die Quantenmechanik der Elektronen in Kristallgittern (About quantum mechanics of electrons in crystal lattices), *Z. Phys.* 52 (7–8) (1929) 555–600.
- [37] B.R. Mace, E. Manconi, Modelling wave propagation in two-dimensional structures using finite element analysis, *J. Sound Vib.* 318 (4) (2008) 884–902.
- [38] M. Ruzzene, F.L. Scarpa, A general FEM technique to model wave propagation in cellular periodic structures, in: *Proc. SPIE 5053, Smart Structures and Materials 2003: Active Materials: Behavior and Mechanics*, vol. 5053, 2003, pp. 414–422.
- [39] R. Langley, A note on the force boundary conditions for two-dimensional periodic structures with corner freedoms, *J. Sound Vib.* 167 (2) (1993) 377–381.
- [40] Polytec GmbH, Polytec-Platz 1-7, 76337 Waldbronn, Germany, Theory Manual Polytec Scanning Vibrometer PSV Theory, as of Software 9.1 Edition.
- [41] M. Abele, K. Bendel, A. Gerlach, M. Liebler, Schallwandler mit zumindest einem Piezoelement ((Ultrasonic transducers with at least one piezo element), German Patent: DE1020110062990A1 (June 2012).
- [42] Dassault Systemes, Abaqus 2017 Online Documentation - Abaqus Analysis User's Guide, 2017.
- [43] P. Langer, M. Maeder, C. Guist, M. Krause, S. Marburg, More than six elements per wavelength: the practical use of structural finite element models and their accuracy in comparison with experimental results, *J. Comput. Acoust.* 25 (4) (2017) 1750025.
- [44] M.W. Hooker, Properties of PZT-Based Piezoelectric Ceramics between -150 and 250°C, Tech. rep., NASA Langley Research Center, 1998.
- [45] E. Heinonen, J. Juuti, S. Leppävuori, Characterization and modelling of 3D piezoelectric ceramic structures with ATILA software, *J. Eur. Ceram. Soc.* 25 (12) (2005) 2467–2470 electroceramics IX.
- [46] Stratasys Ltd, Material Data Sheet - VeroWhitePlus (RGD835), 2016.
- [47] Stratasys, Design with Brilliance - Game-Changing Versatility and Realism with the World's Most Advanced Full-Color Multi-Material 3D Printer, 2017.
- [48] Deutsches Institut für Normung, (German Institute for Standardization), DIN 1320 Akustik Begriffe (Acoustical Terms), Dec. 2009.